Drosophila roadblock and *Chlamydomonas* LC7: A Conserved Family of Dynein-associated Proteins Involved in Axonal Transport, Flagellar Motility, and Mitosis

Aaron B. Bowman,* Ramila S. Patel-King,§ Sharon E. Benashski,§ J. Michael McCaffery,‡ Lawrence S.B. Goldstein,* and Stephen M. King§

*Howard Hughes Medical Institute, Division of Cellular and Molecular Medicine, Department of Pharmacology, University of California San Diego, La Jolla, California 92093-0683; ‡Integrated Imaging Center, Department of Biology, Johns Hopkins University, Baltimore, Maryland 21218; and §Department of Biochemistry, University of Connecticut Health Center, Farmington, Connecticut 06032-3305

Abstract. Eukaryotic organisms utilize microtubule-dependent motors of the kinesin and dynein superfamilies to generate intracellular movement. To identify new genes involved in the regulation of axonal transport in *Drosophila melanogaster*, we undertook a screen based upon the sluggish larval phenotype of known motor mutants. One of the mutants identified in this screen, *roadblock* (*robl*), exhibits diverse defects in intracellular transport including axonal transport and mitosis. These defects include intra-axonal accumulations of cargoes, severe axonal degeneration, and aberrant chromosome segregation. The gene identified by *robl* encodes a 97–amino acid polypeptide that is 57% identical (70% similar) to the 105–amino acid *Chlamydomonas* outer arm dynein–associated protein LC7, also reported here. Both robl and LC7 have homology to several other genes from fruit fly, nematode, and mammals, but not *Saccharomyces cerevisiae*. Furthermore, we demonstrate that members of this family of proteins are associated with both flagellar outer arm dynein and *Drosophila* and rat brain cytoplasmic dynein. We propose that roadblock/LC7 family members may modulate specific dynein functions.

Key words: axonal transport • mitosis • dynein ATPase • nerve degeneration • flagella

Intracellular transport is facilitated by the movement of cytoplasmic dyneins and kinesins along ordered arrays of microtubules (Hirokawa, 1998). For example, plus end–directed kinesins move axonal cargo in the anterograde direction, whereas minus end–directed kinesins and cytoplasmic dynein generate the movement of retrograde axonal traffic. The motions of chromosomes in mitosis are also mediated by the actions of these motors on an ordered array of microtubules, the mitotic spindle apparatus. While multiple motors have been identified in both systems, and in some cases cargoes determined, little is known about the regulation of the movement they drive. Perhaps, the largest roadblock to answering these questions is the identification of proteins involved in these processes.

Address correspondence to Lawrence Goldstein, Howard Hughes Medical Institute, Division of Cellular and Molecular Medicine, Department of Pharmacology, 334 m/c 0683, University of California San Diego, La Jolla, CA 92093-0683. Tel.: (619) 534-9702. Fax: (619) 534-9701. E-mail: lgoldstein@ucsd.edu

Reprint requests may be sent to either L.S.B. Goldstein or S.M. King.

Dyneins, in particular, pose an important challenge because of the large numbers of associated proteins and diverse structural and functional roles (for review see Milisav, 1998). For example, in axonemes the outer arms and one class of inner arm contain two or more heavy chains (~530 kD) that form the globular heads and stems of the particle and provide the sites of ATP hydrolysis and microtubule motor activity. These heavy chains are tightly associated with one or more light chains that may directly regulate motor function (for example in response to Ca^{2+}; King and Patel-King, 1995a). The base of the outer arm dynein particle consists of an additional subcomplex comprised of two closely related intermediate chains that contain WD repeats. At least one of these intermediate chains appears to be involved in cargo binding within the flagellum. Several additional light chains, some of which are shared between different dynein classes and are essential for dynein assembly, are found at the base of the outer arm dynein.

Cytoplasmic dynein is similarly complex and consists of a homodimer of heavy chains, a dimer of a WD repeat intermediate chains, four light intermediate chains (not

present in the outer dynein arm), and several light chains. The 74-kD cytoplasmic dynein intermediate chain (IC74)[1] has been shown to mediate the dynein–dynactin interaction via direct association with $p150^{glued}$ (Karki and Holzbaur, 1995). Dynactin is a multisubunit complex that may play a role in organelle transport and dynein subcellular localization (for review see Holleran et al., 1998). However, the regulation and role of this dynein–dynactin interaction within the context of dynein function is not clear.

Recent work suggests that dynein light chains (DLCs) may play crucial roles in dynein function and regulation. To date, two classes of cytoplasmic DLCs have been identified including Tctex1 (and the homologous rp3) and the highly conserved 10 kD/LC8 DLC (previously called the M_r 8,000 light chain). Both classes are also found associated with axonemal dynein. Tctex1 is a cytoplasmic and inner arm DLC thought to be involved in the meiotic drive of mouse *t*-haplotypes (King et al., 1996b; Harrison et al., 1998; Kagami et al., 1998). Tctex1 also appears to associate with a subset of cytoplasmic dynein localized predominantly to the Golgi apparatus, its tissue distribution is quite distinct from that of the related light chain rp3 (King et al., 1998; Tai et al., 1998). The 10 kD/LC8 DLC, associated with both cytoplasmic dynein and outer arm dynein (King and Patel-King, 1995b; King et al., 1996a), is also found associated with other enzyme systems such as myosin V (Espindola, F.S., R.E. Cheney, S.M. King, D.M. Suter, and M.S. Mooseker. 1996. American Society of Cell Biology. 372a (Abstr.)), neuronal NOS (Jaffrey and Snyder, 1996), and IκBα (Crepieux et al., 1997). Mutations in *Drosophila* lead to altered axon trajectories, female sterility, morphogenetic defects, and apoptotic cell death (Dick et al., 1996; Phillis et al., 1996). This light chain is also essential for dynein heavy chain localization and nuclear migration in *Aspergillus* and for retrograde intraflagellar transport in *Chlamydomonas* (Beckwith et al., 1998; Pazour et al., 1998). Although the basis for dynein's requirement for numerous associated light chains remains obscure, it has become apparent that these proteins play numerous roles in dynein function.

To identify novel modulators of kinesin and dynein motor function, we took advantage of the observation that mutations in axonal transport motors of *Drosophila* share a common larval phenotype of posterior sluggishness and axonal cargo accumulation (Hurd and Saxton, 1996; Gindhart et al., 1998). Based upon these phenotypes we carried out a mutant screen in *Drosophila melanogaster*. Here we report the cloning of one such mutant identified in this screen, *roadblock* (*robl*). In a complementary approach to understanding the regulation of dynein motors, we cloned the gene for the LC7 polypeptide associated with outer dynein arms from *Chlamydomonas* axonemes and found it to be highly homologous to robl. Together, these data identify a new family of dynein-associated proteins (both axonemal and cytoplasmic) with a role in the microtubule-based processes of axonal transport, flagellar motility, and mitosis.

1. *Abbreviations used in this paper:* BDGP, Berkeley *Drosophila* Genome Project; bxd, late RNA encoded bithoraxoid protein; ChAT, choline acetyltransferase; DLC, dynein light chain; EMS, ethyl methanesulfonate; EST, expressed sequence tag; IC74, 74-kD cytoplasmic dynein intermediate chain; khc, kinesin heavy chain; NCBI, National Center for Biotechnology Information; robl, *roadblock*; SYT, synaptotagmin; VG, ventral ganglion.

Materials and Methods

Axoneme and Dynein Purification

Flagella were isolated from wild-type *Chlamydomonas* by standard methods (Witman, 1986) and demembranated with NP-40. Dyneins were extracted with 0.6 M NaCl and further purified by sedimentation through a 5–20% sucrose gradient (King et al., 1986). Flagellar axonemes were also prepared from mutants lacking outer (*oda9*) and various subsets of inner (*ida1-4*) dynein arms.

Rat brain cytoplasmic dynein was isolated by ATP-dependent microtubule affinity (Paschal et al., 1991) and was further purified by sucrose density gradient centrifugation. Alternatively, cytoplasmic dynein, dynactin, and kinesin were obtained directly from rat brain homogenates by immunoprecipitation using the 74-1, 50-1, and H-2 mAbs, respectively, as described previously (Dillman and Pfister, 1994; King et al., 1996a). These samples were provided by Dr. Kevin Pfister (University of Virginia Health Science Center).

Drosophila dynein was immunoprecipitated from 0–15 h embryo homogenates with the 74-1 antibody using a method similar to the one above. In brief, 0.6 g (wet weight) of dechorionated embryos were homogenized in 1 ml of lysis buffer (25 mM Tris-Cl, pH 8.0, 50 mM NaCl, 0.5% Triton X-100, 2 mM EDTA, 1 mM PMSF) containing 10 μg/ml aprotinin, 40 μg/ml bestatin, and 1 μg/ml leupeptin. The homogenate was split into two 400 μl aliquots to which 2.5 μg of 74-1 antibody was added to one sample (dynein immunoprecipitate), the other was mock-immunoprecipitated without antibody (bead control). Precipitation was performed with 10 μl of protein A–Sepharose 4B (Zymed Labs, Inc.) preblocked with 5% BSA in lysis buffer. The beads were washed five times with 20 vol of lysis buffer and the final immunoprecipitate was resuspended in 50 μl of SDS-PAGE loading buffer. 20 μl of each pellet were analyzed by Western blot as described below.

Chlamydomonas axoneme and rat brain dynein samples were electrophoresed in 5–15% acrylamide gradient gels. *Drosophila* samples were electrophoresed with tricine buffer in 10% acrylamide gels. The gels were either stained with Coomassie blue or blotted to nitrocellulose and probed with the 74-1 mAb to detect IC74 (Dillman and Pfister, 1994); *Chlamydomonas* and rat samples were also probed with R7178 rabbit polyclonal antibody anti-LC7 (1:50), see below, whereas *Drosophila* samples were probed with 6883 rabbit polyclonal antibody anti-robl (1:500), see below, or with the anti-tubulin mAb 3A5 (Piperno and Fuller, 1985). Immunoblotting conditions were as previously described (King et al., 1996a).

Analysis of Peptides from LC7

Purified outer arm dynein was concentrated in a Centricon 30 ultrafiltration unit (Amicon) that had been previously treated with 5% Tween 20 in TBS to reduce nonspecific protein binding. The sample was electrophoresed in a 5–15% acrylamide gradient gel and blotted to a polyvinylidene difluoride membrane (Immobilon P^{sq}; Millipore Corp.). The LC7 band was excised and treated with trypsin in situ. Peptides eluting from the membrane were purified by reverse-phase chromatography using a C_8 column and peptide masses determined by matrix-assisted laser desorption/ionization time-of-flight mass spectrometry. Two peptides of sufficient purity were obtained and sequenced at the Protein Microsequencing Facility, University of Massachusetts Medical School.

Molecular Analysis of LC7

A portion of the LC7 coding region (~450 bp) was originally obtained from the first strand of cDNA made from RNA enriched for flagellar sequences using PCR. The forward primer 5′-GCGCGAATTCAAGAAGCACGAGATYATG-3′ was designed from the peptide sequence (K)KHEIM using the *Chlamydomonas* codon bias and incorporated an EcoRI site and GC clamp at the 5′ end. The oligo (dT) adaptor 5′-GCGCGTCGACTCGAGT_{20}V-3′ was employed as the reverse primer. The reaction was performed using Pfu DNA polymerase and standard buffer conditions with the following thermal profile: 96°C for 1 min, 50°C for 1 min, and 72°C for 1 min for 40 cycles followed by a final 10 min at 72°C. This PCR product was used to isolate a full-length clone from a λZapII *Chlamydomonas* cDNA library. Multiple clones were obtained

and the longest sequenced on both strands using Sequanase v2.0 and a 7-deaza dGTP sequencing kit (U.S. Biochemical Co.). Southern and Northern blots were prepared and probed using standard methods.

LC7 Fusion Protein and Antibody Preparation

The LC7 coding region was subcloned into the pMAL-c2 vector by PCR-based cloning (New England Biolabs Inc.). This resulted in the COOH-terminal fusion of LC7 to the maltose-binding protein via a hydrophilic linker containing a Factor Xa cleavage site. Expressed protein was purified by amylose affinity chromatography and the entire fusion protein was used to raise antisera in rabbit R7178. Subsequently, electrophoretically isolated recombinant LC7 was used to blot purify the antisera using the minor adaptions to the method of Olmsted (1986) described by King et al. (1996a).

Identification of the roadblock Mutant

F3 lethal balanced ethyl methanesulfonate (EMS) mutant lines (cn bw l(2)EMS/Cyo) were obtained from the laboratory of Dr. Charles Zuker (University of California San Diego). The mutant larvae were examined 5 to 6 d after egg laying for sluggish crawling behavior. *Roadblock* was identified as a posterior larval sluggish mutant with a late third instar larval lethal phase ($robl^{z}$ allele). Preliminary studies identified an absence of imaginal tissue and extreme posterior paralysis in which larvae become completely paralyzed in the posterior, whereas the anterior remained noticeably mobile.

Cloning of the roadblock Gene

The *robl* gene was mapped approximately to cytological position 54 on the second chromosome of *Drosophila* by meiotic recombination. Screening of nearby lethal alleles obtained from the lab of Dr. Gerry Rubin (University of California Berkeley), identified l(2)k10408 as a *robl* allele ($robl^{l(2)k10408}$). Additionally a P-element mobilization screen with other nearby insertions generated another *robl* allele ($robl^{c}$). Genomic sequence was rescued off the ends of $robl^{l(2)k10408}$ and $robl^{c}$ by inverse PCR (BDGP protocol; http://www.fruitfly.org/p_disrupt/) and used to identify *Drosophila* P1 genomic clones from the Berkeley Drosophila Genome Project (BDGP) using the P1 filter blot purchased from Genome Systems, Inc. The P1 clones in the *robl* genomic region (DS02323 and DS02859) were sequenced using an ABI 377 DNA sequencer. Analysis revealed large deletions in $robl^{l(2)k10408}$ and $robl^{c}$ that were partially overlapping, thus, identifying the *robl* genomic interval. Homozygous $robl^{l(2)k10408}$ and $robl^{c}$ genomic DNA were made from third instar larvae and used to confirm both deficiencies by PCR and Southern analysis. Sequencing and PCR analysis of $robl^{z}$ homozygous DNA revealed a 193-bp deletion identifying the *robl* gene. BLAST analysis using the BDGP database identified a full-length expressed sequence tag (EST) clone that encodes robl; this clone (LD34974; accession number AI061910) was ordered from Genome Systems, Inc. Sequence of the ~15-kb *robl* genomic interval and *robl* cDNA has been deposited at National Center for Biotechnology Information (NCBI) GenBank (accession numbers AF141921 and AF141920).

Genomic and cDNA rescue construct lines were generated using standard techniques. The genomic construct (a 6.6-kb SpeI-KpnI fragment) was cloned into pP{CaSpeR 4} and the cDNA construct was cloned into pP{CaSpeR hs-ACT} (provided by Dr. Carl Thummel, University of Utah) by PCR cloning to introduce a 6xHis tag at the NH_2 terminus (adding the amino acids: MGSSHHHHHHSSG). Multiple X chromosome insertion lines were obtained and used to test for rescue. The cDNA rescue construct (which is under control of an HSP70Bb promoter) was induced daily for 1 h at 37°C.

roadblock Fusion Protein and Antibody Preparation

The 6xHis-tagged robl fusion protein used in the cDNA rescue experiments was subcloned into the pET-14b vector by PCR-based cloning (Novagen, Inc.). Expressed protein was purified by Talon Superflow metal affinity resin according to the recommended protocol (CLONTECH Laboratories, Inc.), and then electrophoretically isolated and used to raise antisera in rabbit 6883. 10 mg of $robl^{l(2)k10408}$ homozygous and wild-type second/third instar larvae (wet weight) were extracted with SDS-PAGE loading buffer and analyzed by Western blot to confirm specificity of the anti-robl antibody.

robl/LC7 Sequence Analysis and Protein Comparison

All sequence assembly and protein comparison were performed using the GCG suite of software (Genetics Computer Group) and Sequencher 3.1 software (Gene Codes Corporation). Roadblock/LC7 family members were identified with the *Drosophila* robl sequence using BLASTP against the NCBI dbNR, TBLASTN against the NCBI dbEST, and TBLASTN against the BDGP DNA sequence database. All gene abbreviations here refer to those detailed in Fig. 4. *Drosophila robl22E* (DS01020; accession number AC004276), *robl37BC* (DS00790; accession number AC005127), *robl62A* (DS02734; accession number AC004343), and *robl60C* (DS02336; accession number AC005718) were identified in BDGP genomic sequence and are apparently intronless genes, just like the related late RNA from the *Bithoraxoid complex* (accession number M27999). EST clones have been identified for late RNA-encoded bithoraxoid protein (bxd) (GH08635; accession number AI113381) and *robl62A* (GH15530; accession number AI292590) by BDGP from a *Drosophila* head cDNA library. The proteins T24H10.6 (accession number 995857) and bxd (accession number 290293) were identified from dbNR using BLASTP. Mouse, rat, and human ESTs identified, were compared by nucleotide sequence using TBLASTN against the species-specific NCBI GenBank dbEST to identify ESTs from identical genes; two different genes were identified in all three species (accession numbers from representative ESTs are given in Fig. 4). The predicted translation of all mammalian ESTs was determined using DNA Strider (CEA); the small size of the genes meant that almost all ESTs translated into full-length protein. Protein comparison was done using the GCG PILEUP command to generate the dendrogram; the output MSF file was run through the BOXSHADE SERVER (http://www.isrec.isb-sib.ch/software/BOX_form.html) and the output EPS file was imported into Adobe Illustrator 6.0.

Larval Segmental Nerve Immunostaining

Larval segmental nerve immunostaining was done as described by Hurd and Saxton (1996). Anti-synaptotagmin (DSYT2) (Littleton et al., 1993) was used at 1:500. Anti-choline acetyltransferase (4B1) (Yasuyama et al., 1995) was used at 1:2,000. Immunostained larvae were observed using a Bio-Rad MRC1024 confocal microscope as previously described (Gindhart et al., 1998).

Electron Microscopy of Larval Segmental Nerves

The method below is a hybrid of our standard protocol (McCaffery and Farquhar, 1995) with a previously described *Drosophila* method (Hurd and Saxton, 1996). *Drosophila* larvae were dissected and pinned open to expose the segmental nerves and muscles. The larvae were fixed for 1 h in 100 mM cacodylate buffer, pH 7.4 at room temperature, containing 3% freshly prepared formaldehyde, 1.5% glutaraldehyde, and 2.5% sucrose. The larvae were washed in 100 mM cacodylate, pH 7.4, containing 2.5% sucrose and subsequently fixed in Palade's osmium (1% OsO_4 prepared in Kellenberger's buffer, pH 6.8) for 1 h on ice. The larvae were enbloc-stained overnight at room temperature in 2% Kellenberger's uranyl acetate, subsequently dehydrated through a graded series of ethanol, and embedded in Epon. Larvae were flat embedded and oriented to permit cross-sectioning and visualization of the larval segmental nerves. 80-nm sections were cut on a Leica Ultracut E ultramicrotome, collected onto 400 mesh nickle, high transmission grids, poststained in 2% uranyl acetate and lead citrate, and observed in a JEOL 1200 EXII transmission electron microscope.

Larval Mitotic Brain Squash Analysis

Untreated third instar larval brain squash analysis was done as previously described (Gonzalez and Glover, 1993). Also, brains from $robl^{z}$ homozygous larvae were analyzed after colchicine (0.5×10^{-5} M for 105 min) and hypotonic treatment as previously described (Gonzalez and Glover, 1993). The mitotic index was determined by counting the number of prometaphase, metaphase, and anaphase mitotic structures seen in a significant number of defined microscope fields (63× objective with 1.6× ocular).

Results

Identification and Cloning of roadblock

roadblock (robl) was identified in a screen for novel ax-

onal transport mutants in *Drosophila melanogaster*. The *robl*^{z} EMS mutant allele is recessive lethal, dying at the third larval instar. The *robl*^{z} homozygous larvae show a progressive posterior sluggish phenotype leading to complete posterior paralysis, a common phenotype of axonal transport mutants in *Drosophila* (Hurd and Saxton, 1996; Gindhart et al., 1998). Further characterization of *robl*^{z} revealed a complete absence of imaginal tissue, indicating a possible strong mitotic defect as well. To obtain *robl* null alleles, deletions were generated from flanking P-elements that mapped near *robl*. Homozygous null and *robl*^{z}/null (*robl*^{z} hemizygote) animals die as late pupae; they also demonstrate a posterior larval sluggishness, a peculiar tail flipping phenotype, and accumulations of axonal cargo within their segmental nerves, as has been described for other axonal transport mutants in *Drosophila* (Hurd and Saxton, 1996; Gindhart et al., 1998). Additionally, the reduced size of imaginal tissue, rough pupal eyes, and missing bristle phenotypes seen in these animals are characteristic of mitotic mutants in *Drosophila*. Thus, the *robl* mutant phenotypes suggest roles for this gene in both axonal transport and mitosis.

Two overlapping deficiencies, *robl*$^{l(2)k10408}$ and *robl*^{c}, identify the genomic interval encoding *robl* (Fig. 1 A). Sequencing of the entire genomic interval identified five putative gene candidates that may be affected by both deficiencies. To identify which gene encoded *robl*, we sequenced *robl*^{z} and discovered a 193-bp deletion in the middle of a small transcription unit in the interval that we believe to be *robl* for several reasons. First, a 5-kb segment of this region that contains only *robl*, and one adjacent gene, was found to fully rescue all above-mentioned phenotypes in *robl*^{z} hemizygotes. Second, this gene adjacent to *robl* was sequenced from *robl*^{z} and found to be unaltered from the wild-type parental chromosome. In fact, this gene appears to be a *robl* pseudogene because it lacks any identifiable start codon. Third, *robl*$^{l(2)k10408}$ homozygotes are fully rescued by the genomic rescue construct that indicates that other genes in this interval are not essential and the observed phenotypes are *robl*-dependent.

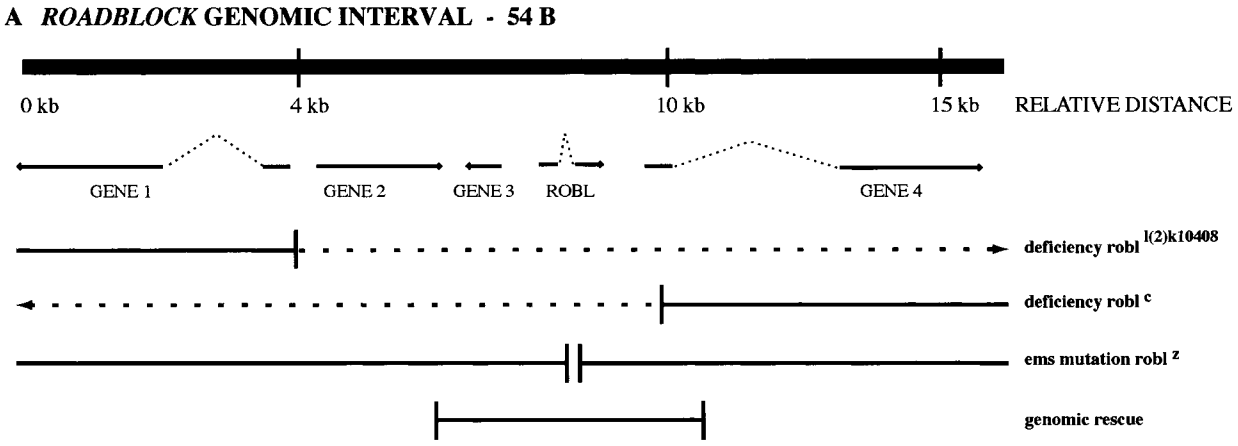

B GENOMIC SEQUENCE ENCODING ROADBLOCK

```
aaaattataagaaaaaATGgtaagtaagagttgtgcatacacaaaaacattaagaaaataacgttaccttcatggcttacagTCGCAGGAGGTTGAGGAAACACTCAAGAGAATCC
               M                              intron 1                                S  Q  E  V  E  E  T  L  K  R  I  Q

AGAGCCACAAAGGTGTTGTGGGTACAATTGTGGTCAACAATGAAGgtgggtggttcaactgcacctcagtgtgtgctaagatatctaactaattctcaacgccttccaaatagGTA
  S  H  K  G  V  V  G  T  I  V  V  N  N  E  G                intron 2                                                  I

TTCCGGTCAAATCCACGCTGGACAACACTACCACCGTTCAGTACGCTGGCCTAATGAGTCAGCTGGCGGACAAGGCACGAAGTGTGGTGAGGGACTTGGATCCTTCCAACGACATG
  P  V  K  S  T  L  D  N  T  T  T  V  Q  Y  A  G  L  M  S  Q  L  A  D  K  A  R  S  V  V  R  D  L  D  P  S  N  D  M

ACATTCCTGCGGGTGCGATCCAAGAAGCACGAGATCATGGTGGCACCCGACAAGGACTTCATCCTGATTGTCATCCAAAACCCAACCGACTAAatggcatggtgcatcgcgactat
T  F  L  R  V  R  S  K  K  H  E  I  M  V  A  P  D  K  D  F  I  L  I  V  I  Q  N  P  T  D  *
```

Figure 1. The *robl* genomic interval. (A) A diagrammatic map of the five genes identified in the genomic region around *roadblock* (accession number AF141921). The entire region has been sequenced and cDNAs have been obtained for *robl* and genes 1 and 4. Gene 3 is a roadblock-like region, which is likely a pseudogene as it lacks any identifiable start codon. The two partially overlapping deficiencies *robl*$^{l(2)k10408}$ and *robl*^{c} identify the *roadblock* genomic region, dotted lines correspond to regions missing in deficiencies. The EMS mutant *robl*^{z} deleted a small region in one of these genes allowing us to identify it as *robl*. The genomic rescue region shown completely rescues *robl*^{z}/*robl*$^{l(2)k10408}$. (B) The genomic sequence of the region encoding *roadblock* (corresponding to nucleotides 7,751–8,214 of genomic interval illustrated in A). Uppercase characters show the protein coding sequence that is translated below for each codon; lowercase characters are used to show the 5′-UTR, introns 1 and 2, and 3′-UTR. The EMS mutant *robl*^{z} has a 193-bp deletion that is represented by bold characters. The deletion extends from intron 2 into the COOH terminus encoding exon 3, removing the intron's conserved branch point sequence that is underlined. Since *robl*^{z} is a recessive neomorphic allele, a partially functional or aberrant protein is likely made. Reverse transcriptase–PCR analysis of *robl*^{z} indicates that splicing of mutant intron 2 does not occur (data not shown). However, the mutant transcript maintains the correct reading frame through the remainder of intron 2 and exon 3. The resulting *robl*^{z} protein would have an internal deletion of 54 residues (IPVKST...HEIMVA) replaced by a 12-residue insertion (GWFNCTSVCAKI) from the remainder of intron 2.

Finally, an NH_2-terminal His-tagged *robl* cDNA construct under control of the hsp70Bb promoter fully rescues male *robl*^{z} hemizygotes if given daily heat shock. Reducing the frequency of heat shocks results in a restoration of the described *robl* phenotype. This cDNA construct does not rescue an apparent female sterility seen in the rescued *robl*^{z} hemizygotes, despite full rescue of all other observed *robl* phenotypes. Nevertheless, taken together, these data establish that the gene identified by the *robl*^{z} deletion is *roadblock*.

The genomic sequence of *robl* reveals a small three exon gene encoding a 97-residue polypeptide (Fig. 1 B). The 193-bp deletion found in *robl*^{z} removes portions of intron 2 and exon 3. Interestingly, this deletion results in a *robl* allele that is more severe than null alleles. The increased severity of *robl*^{z} homozygous animals compared with *robl*^{z} hemizygotes or homozygous null animals suggests that this internal deletion is a recessive neomorphic allele that poisons intracellular transport. In fact, *robl*^{z} homozygotes cannot be fully rescued by the genomic or cDNA rescue constructs. Thus, two copies of the *robl*^{z} mutation act in a dominant fashion to inhibit the action of wild-type *robl*. An alternative explanation for the inability to rescue *robl*^{z} homozygotes would be a secondary lethal lesion on the *robl*^{z} chromosome. However, we have confirmed the absence of any other lethal complementation groups on the *robl*^{z} chromosome by recombination mapping (data not shown).

Chlamydomonas LC7 Is an Outer Arm Dynein-associated Protein

The *Chlamydomonas* outer dynein arm contains eight distinct light chain components (Piperno and Luck, 1979; Pfister et al., 1982). Previously, we cloned and described all of these proteins except for LC7. To clone LC7, we purified and sequenced two tryptic LC7 peptides isolated from outer arm dynein (Fig. 2 A). Based upon this sequence, PCR primers were designed and an LC7 cDNA clone isolated. The largest cDNA clone was 864 bp in length (Fig. 2 B) and contained a single open reading frame of 105 residues with a predicted mass of 11,928 D and a calculated pI of 7.85. Both peptide sequences obtained from purified LC7 were found in this clone (26/26 residues correct) and were both preceded by the predicted basic residue. Three in frame stop codons were present up-

A

PEPTIDE SEQUENCE	CALCULATED MASS (DA)	ACTUAL MASS (DA)
KHEIMIAPEFER	1500	1516*
SHEYYLVVVQDPSR	1692	1692

* INCLUDES METHIONINE OXIDATION PRODUCT.

B

```
  1 TGCGGACATACCTTTGCAACATTAGGTAAACATTAGCAGAAAACATTAGCCACACGCGTT  60
 61 GACGATTCCTCACAGCTCCGAGAGACCAACCTGAATCTCGAGAATGGTCGACATTGCCGC 120
  1                                    M  V  D  I  A  A            6

121 TGTCGATGAGACATTCAAGCGTCTGCAAAGCCACAAGGGCGTACTAGGGATCATTGTCAT 180
  7  V  D  E  T  F  K  R  L  Q  S  H  K  G  V  L  G  I  I  V  I   26

181 CAACGCGGAGGGAATTGCTATCCGCACGACCTTTGACAACGACCTGACCGTCCAGTACGC 240
 27  N  A  E  G  I  A  I  R  T  T  F  D  N  D  L  T  V  Q  Y  A   46

241 GGCCCTGGTCTCGCACTTCACCGTCAAGGCGCGCTCAGCTGTGCGGAAACTGGATGGGGA 300
 47  A  L  V  S  H  F  T  V  K  A  R  S  A  V  R  K  L  D  G  D   66

301 TAACGACCTCAAGTTCCTGCGGATACGTTCCAAGAAGCACGAAATTATGATTGCGCCAGA 360
 67  N  D  L  K  F  L  R  I  R  S  K  K  H  E  I  M  I  A  P  E   86

361 GTTTGAGAGGTCGCATGAATACTATCTGGTCGTGGTGCAAGACCCCTCACGAGAGGCGTG 420
 87  F  E  R  S  H  E  Y  Y  L  V  V  V  Q  D  P  S  R  E  A  *  105

421 AGATGGCATAGGCGGGTGCGGAGGCGCTAGCGGCGATTCAGCTTGCGTGGCATGCGCCTG 480
481 GCCACAAGGGGCCGCTTGATAACGCGGCATGTATCCATTCTGTTAGTTAGGACTATTGCC 540
541 GGCCGGGGAGCGGGCGGCGCTCGCGAAGGGGGAGTTATAGGTGCAAGGAGTTAGCTGCCT 600
601 TGCACAAGGTCGTGGGGAGAAGCCCCCAGGCTGGCCGTGGTTGGACCTTGGGGCCTGGGA 660
661 CTGCTGGACGTGTGAAGCAGCTGCAGGTTGCTGCAGCTGCACCGCTTATGTACATAACAG 720
721 ATGCAGATGATGGAGAGGAGAAGGTGGCTTGCAGACAAATGCAAGGACACAAAGCTTGTC 780
781 TGTGGGCGTGGCATGTCACACGGGGCTTCCGTCGCTCAGACCCCTGTAAACGTAACGGTG 840
841 AAAAAAAAAAAAAAAAAAAAAAA 864
```

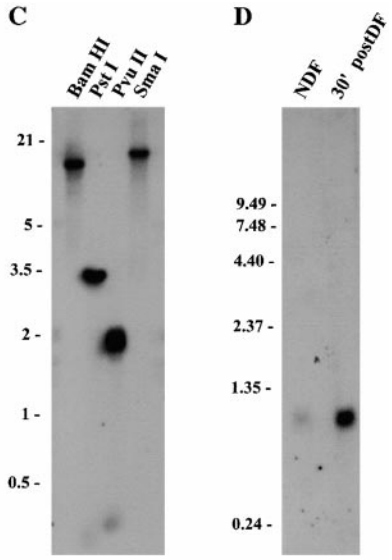

Figure 2. Molecular analysis of LC7 from the *Chlamydomonas* outer dynein arm. (A) Two tryptic peptides from outer arm dynein LC7 were completely sequenced, yielding a total of 26 residue assignments. The actual mass of each peptide is in agreement with the calculated mass once methionine oxidation of the upper peptide is incorporated. (B) DNA and predicted protein sequence for the *Chlamydomonas* LC7 cDNA clone. Both peptide sequences are found in the coding region (26/26 residues correct). These sequences are indicated in bold type and are contiguous in the primary structure. The polyadenylation signal is underlined. This sequence is available in the NCBI GenBank (accession number AF140239). (C) Southern blot of genomic DNA from *Chlamydomonas* strain S1D2 digested with BamHI, PstI, PvuII, and SmaI and probed with the full-length LC7 cDNA. The data suggest that there is a single gene for LC7 in *Chlamydomonas*. (D) Northern blot analysis of RNA from nondeflagellated cells and from those actively regenerating flagella (30′ postDF). A single message of ~0.95 kb that is induced in regenerating cells is evident.

stream of the first Met residue and a 489-bp 3′ untranslated region, including a perfect copy of the *Chlamydomonas* polyadenylation signal, followed the stop codon.

Genomic Southern blot analysis revealed a single band in both BamHI- and SmaI-digested DNA, suggesting that there is a single LC7 gene in *Chlamydomonas* (Fig. 2 C). As is characteristic of flagellar proteins, Northern analysis revealed one message of ~0.95 kb that was greatly upregulated in cells that were actively regenerating their flagella (Fig. 2 D).

The outer arm dynein samples used to obtain LC7 peptide sequences also contained inner dynein arm I1. This dynein partially cofractionates with the outer arm and is now known to contain light chain components (Harrison et al., 1998). To confirm that the LC7 protein is a component of the outer arm, axonemes were prepared from mutants lacking specific dynein structures including the outer arm (*oda9*), inner arm I1 (*ida1*, *ida2*, and *ida3*), and a subset of inner arms I2/3 (*ida4*). Immunoblot analysis of these samples using a polyclonal LC7 antiserum revealed that the LC7 polypeptide was present in the mutants lacking inner arms, but was drastically reduced in the strain lacking outer arms (Fig. 3 A). Upon overexposure of the blot, a very small amount of LC7 could be detected in the outer armless axonemes. The origin of this minor fraction remains unclear as the LC7 protein could not be detected in sucrose gradient profiles of high salt extracts from outer armless strains (data not shown). Furthermore, sucrose gradient analysis of extracts from wild-type axonemes revealed that all the extracted LC7 comigrated with the outer arm at ~18 S (Fig. 3 B).

A Family of robl/LC7 Proteins Is Conserved from Nematode to Man

The cloning of roadblock and LC7 revealed these proteins to be 57% identical and 70% similar. Additionally, both proteins are related to the predicted protein sequence from the late RNA of the *Drosophila bithoraxoid complex* (bxd); robl is 30% identical and 42% similar to bxd; LC7 is 26% identical and 39% similar to bxd. However, no known function has been attributed to this coding transcript from *bxd* (Lipshitz et al., 1987). The robl/LC7 similarity prompted us to look for additional robl-like genes in the NCBI GenBank. BLAST and comparative protein sequence analysis identified a large family of robl-like proteins conserved in *Drosophila*, nematode, *Chlamydomonas*, and three mammalian species (Fig. 4, A and B). Four other robl-like genes, in addition to the *bxd* late RNA, were identified in *Drosophila* and are designated here by their cytological location: *robl62A*, *robl37BC*, *robl22E*, and *robl60C*. In mammals, two classes of robl/LC7-like genes were identified by homology (Fig. 4 A). However *C. elegans* apparently has only a single robl-like gene in its genome (Fig. 4 A). The differences between robl/LC7-like family members may suggest a possible functional distinction between the various members within an organism.

robl Mutants Have a Distal Biased Axonal Transport Defect

Mutations in *robl* cause phenotypes similar to other axonal transport mutants in *Drosophila*. Previous analysis of kinesin heavy chain (khc) and kinesin light chain mutants demonstrated massive accumulations of axonal cargo and motors distributed randomly along the entire length of the larval segmental nerves. These accumulations were shown to be massive local axonal swellings that fill with organelles and vesicles (Hurd and Saxton, 1996; Gindhart et al., 1998). The accumulation phenotype correlates with the other common axonal transport phenotypes in *Drosophila*, tail flipping and posterior paralysis. It was proposed that these mutants disrupt the processive movement of their cargo

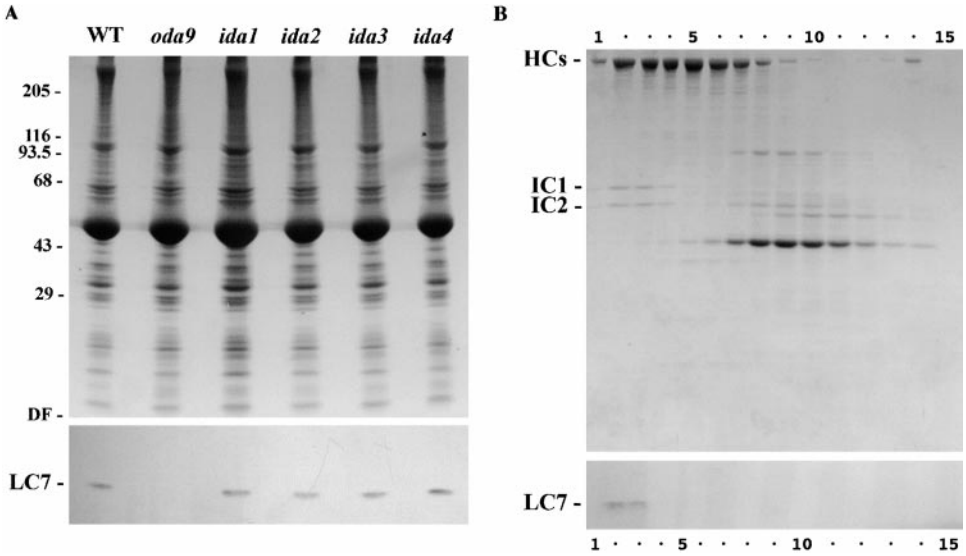

Figure 3. LC7 is a component of the outer dynein arm. (A) Flagellar axonemes were prepared from wild-type *Chlamydomonas* (*WT*) and from mutants lacking the outer arm (*oda9*), inner arm I1 (*ida1*, *ida2*, and *ida3*), and inner arms I2/3 (*ida4*). Samples were electrophoresed in a 5–15% acrylamide gradient gel and either stained with Coomassie blue (upper panel) or blotted to nitrocellulose and probed with the R7178 antibody to detect LC7. The LC7 protein is highly reduced only in the strain lacking outer dynein arms. (B) A high salt extract of wild-type axonemes was sedimented through a 5–20% sucrose gradient and fractions electrophoresed in 5–15% acrylamide gels. Fraction 1 is the bottom of the gradient. The upper panel shows the gel stained with Coomassie blue, the lower panel is an immunoblot probed with R7178 to detect the LC7 protein. All the salt extractable LC7 protein precisely comigrates at ~18 S with components of the outer dynein arm (e.g., IC1 and IC2).

A ROADBLOCK/LC7 FAMILY DENDROGRAM

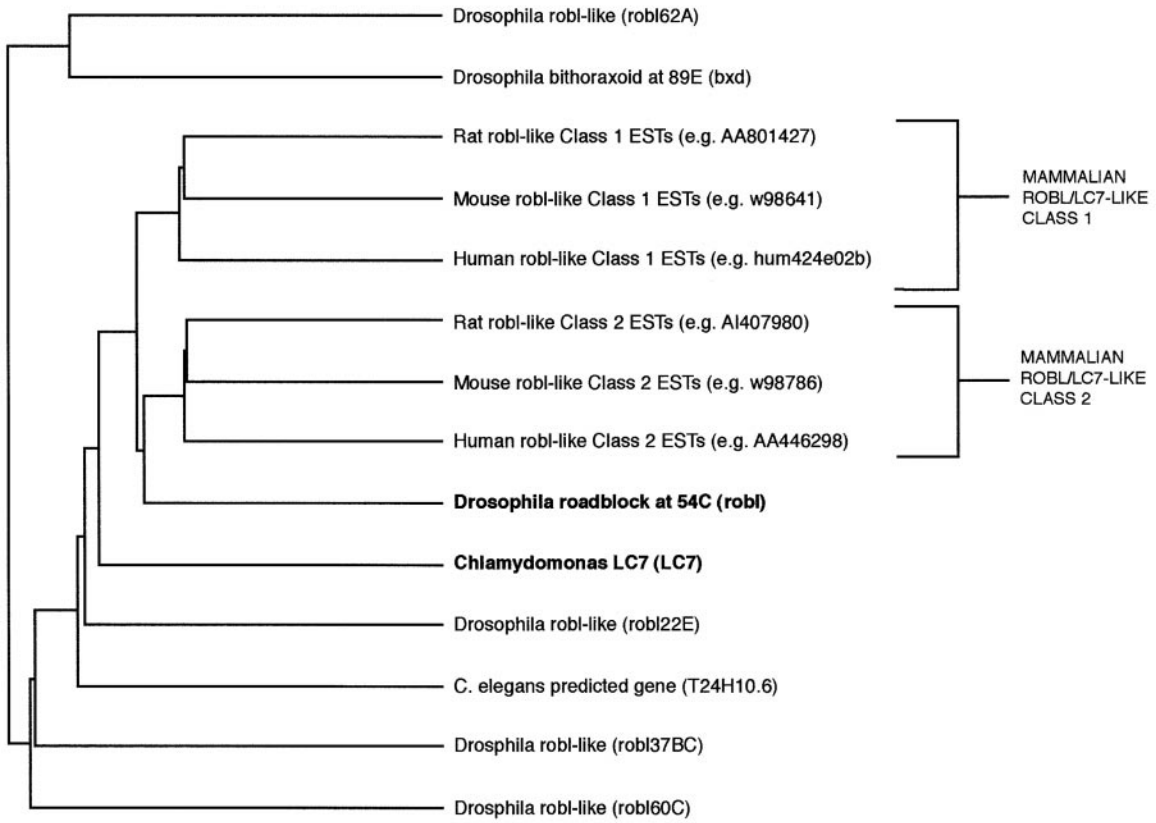

B ROADBLOCK/LC7 FAMILY ALIGNMENT

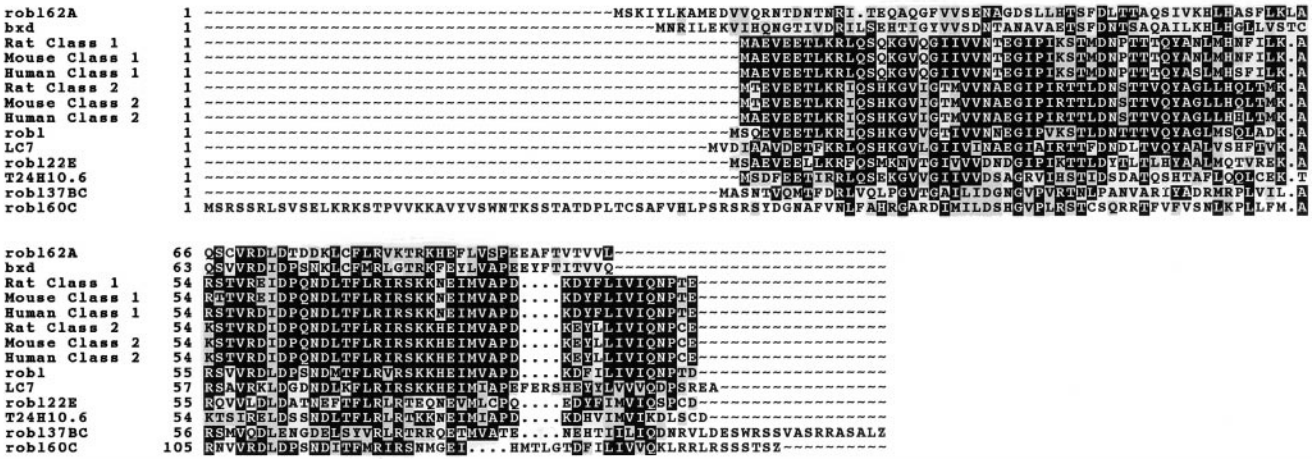

Figure 4. A large family of robl/LC7-like proteins. BLAST analysis has identified several mammalian ESTs, *Drosophila* genes, and a gene from *C. elegans* that are highly homologous to robl/LC7. (A) A dendrogram of the robl/LC7-like family members identified is shown. This dendrogram was generated using the GCG PILEUP command. We identified at least five *Drosophila* roadblock-like genes by searching the BDGP-derived ESTs and genomic sequences. Previously unidentified genes have been designated by their cytological location determined by BDGP. Also, two classes of robl/LC7-like genes have been identified as mammalian ESTs (identified by a representative EST accession number). (B) An alignment of the protein family is shown. The alignment was generated by the same GCG PILEUP command as an MSF file. BOXSHADE was used to illustrate aligned amino acid identity (dark shaded residues) and similarity (light shaded residues).

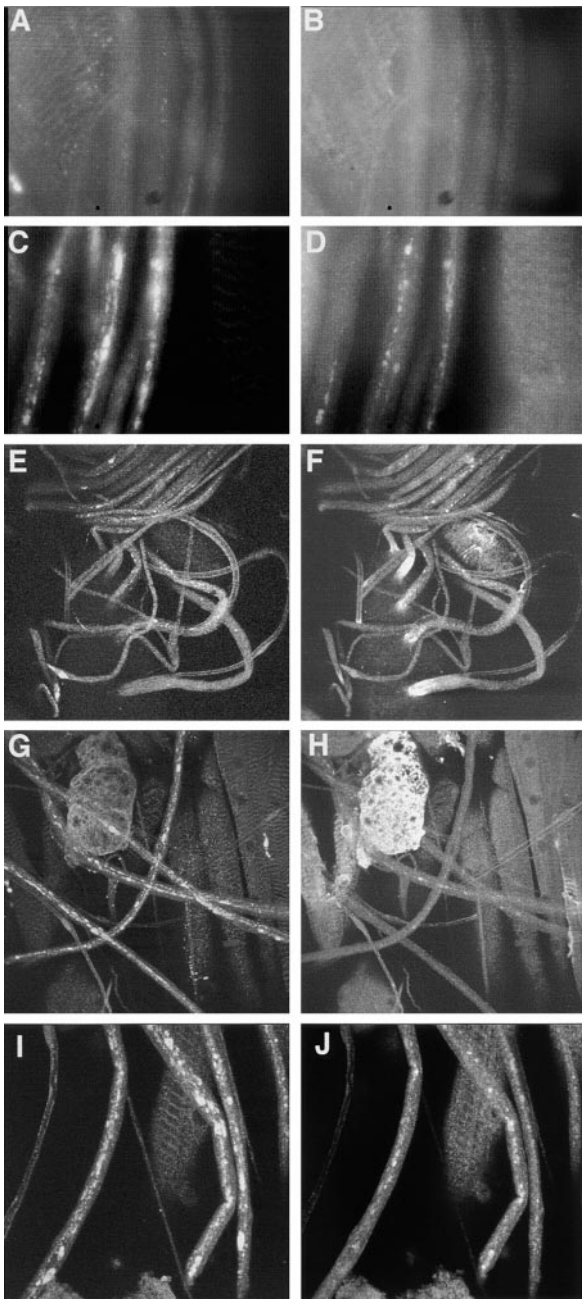

Figure 5. Coimmunostaining of larval segmental nerves for (left column) SYT and (right column) ChAT revealed distal axonal accumulations of synaptic cargo in *robl* mutants. (A and B) In wild type, there is only a low background staining observed. (C and D) Segmental nerves from *robl*^{z} hemizygotes have accumulations of SYT and ChAT. (E and F) In *robl*^{z} hemizygotes the segmental nerves at the anterior, coming off of the ventral ganglion (located at the bottom left quadrant in images E and F), show a decreased frequency of SYT accumulations but an increased frequency of ChAT accumulations when compared with more posterior regions. (G and H) The segmental nerves located at the posterior show an increased frequency of SYT accumulations with a corresponding decreased frequency of ChAT accumulations. (I and J) Segmental nerves from *robl* null homozygotes (*robl*^{k}/*robl*^{k}) show abundant accumulations of SYT and ChAT.

within the axon, causing the axons to swell, filling with transported axonal material. Immunostaining of *robl*^{z}/null hemizygous and *robl* null homozygous larvae reveals frequent accumulations of synaptotagmin (SYT) (Fig. 5, C and I) and choline acetyltransferase (ChAT) (Fig. 5, D and J) in the larval segmental nerves. In contrast, SYT (Fig. 5 A) and ChAT (Fig. 5 B) show only a low background level staining in wild-type segmental nerves. Additionally, axonal transport motors (of the kinesin I and kinesin II family), cysteine string protein, and a marker for endocytic traffic are also observed to accumulate in the axons of *robl* mutants (data not shown). Thus, *robl* mutants have a gross phenotype similar to that previously described for axonal transport mutants in *Drosophila*; a progressive larval posterior paralysis, tail flipping, and segmental nerve axonal cargo accumulation.

In *robl*^{z} mutants, unlike previously described axonal transport mutants, there is a strong tendency for the synaptic cargo to accumulate at the distal regions of axons with only infrequent proximal accumulations. This distal bias can be inferred from the organization of the *Drosophila* larval nervous system. The larval segmental nerves are anti-parallel bundles of mostly cholinergic sensory neuron axons and noncholinergic motor neuron axons. The (ChAT and SYT expressing) sensory neurons project axons from peripheral cell bodies towards the anterior into the ventral ganglion (VG), whereas the (SYT expressing but ChAT lacking) motor neurons project axons in the opposite direction from cell bodies in the VG towards the posterior and peripherally where they form neuromuscular junctions.

In *robl*^{z} hemizygous larvae, ChAT accumulations were found predominantly in the distal portions of the sensory axons (the anterior region of the larval segmental nerves) as seen by comparing staining at the anterior VG (Fig. 5 F) with staining observed in segmental nerves in the posterior of the larvae (Fig. 5 H). SYT shows a gradual increase in the frequency of accumulations toward the distal portions of the motor axons (the posterior region of the larval segmental nerves) as seen by comparing the staining at the anterior VG (Fig. 5 E) with staining observed in segmental nerves at the posterior region of the larvae (Fig. 5 G). Thus, the frequency of ChAT accumulations is inversely correlated with the distance from the VG, whereas SYT accumulations show the opposite correlation.

We further analyzed this distal enrichment of axonal accumulations by SYT–ChAT co-immunostaining analysis. Since ChAT is expressed only in sensory neurons, SYT–ChAT co-accumulations can only occur in sensory neuron axons. In addition, most (~95%) of ChAT accumulations along the length of the nerves co-immunostain with SYT, supporting a view that most ChAT negative SYT accumulations occur in motor axons. Co-immunostaining demonstrated that 71% of anterior SYT cargo accumulations are ChAT positive. Thus, most anterior SYT accumulations are occurring in the distal regions of sensory axons and not the proximal region of motor axons. In contrast, only 16% of the posterior SYT accumulations are ChAT positive. Thus, most of the posterior SYT accumulations are likely occurring in the distal regions of motor axons and not the proximal regions of sensory axons. Therefore, the combined observations of an anterior–posterior accumulation

frequency gradient, the majority of anterior SYT accumulations occurring in sensory axons, whereas the majority of posterior SYT accumulations occurring in motor axons, demonstrates that there is a strong propensity for synaptic axonal cargo accumulation to occur in the distal regions of axons in *roadblock* mutants.

Comparative analysis of *robl* null, *robl*^{z} hemizygous, and *robl*^{z} homozygous nerves revealed that as the number of *robl*^{z} alleles is increased, the number of observed SYT and ChAT accumulations decreased. The *robl*^{z} homozygous larvae have fewer axonal accumulations, ranging from ~1–5% than that observed for hemizygotes (data not shown). A similar distal enrichment in accumulations is observed for *robl*^{z} homozygotes, as has been described above for *robl*^{z} hemizygotes. Homozygous *robl* null larvae show a significant increase in axonal accumulations, ranging from ~200–400% than that observed for hemizygotes (data not shown). However, the ChAT accumulations in *robl* null homozygotes appear more uniformly distributed, despite obvious distal-enriched SYT accumulations. Perhaps, the large number of axonal accumulations observed in the *robl* nulls obscures the distal bias; alternatively, sensory neuron axons (ChAT positive axons) may be affected differently in *robl* nulls.

robl Mutants Have Massive Axonal Loss and Nerve Degeneration

We used EM to examine the morphology of the axonal swellings in segmental nerves from *robl* mutants. Previously, transmission EM of larval segmental nerves from *khc* mutants revealed that these massive axonal swellings are filled with all types of identifiable axonal cargo (Hurd and Saxton, 1996). The nerves of *robl*^{z}/null (hemizygote) larvae also contain swollen axons that have become filled with axonal cargo (Fig. 6, A and D). These swollen axons are on average twice the diameter of the largest axon observed in wild type (Fig. 6 B). While the axonal swellings observed in *khc* mutants vary in size, their content characteristics are uniform, containing all observed membrane bound axonal content (Hurd and Saxton, 1996). In addition to these multicomponent axonal accumulations (Fig. 6 D), *robl* mutants also have a small subset of single component axonal accumulations (Fig. 6 C). These single compo-

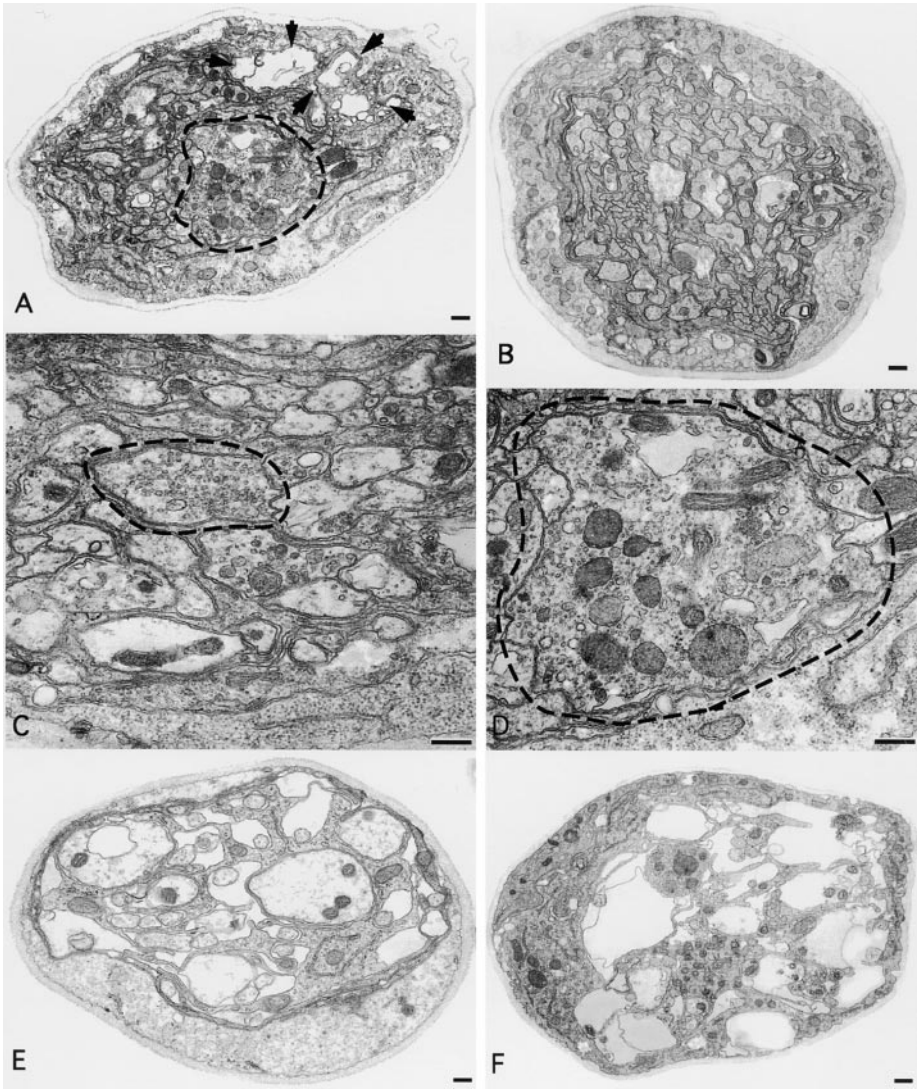

Figure 6. Transmission EM cross-sections of *robl* mutant third instar larval segmental nerves revealed two classes of axonal cargo accumulations and severe axonal loss and nerve degeneration. (A) Nerves from *robl*^{z} hemizygous larvae had axons that swelled with transported material (dashed circles) and showed a loss of axons and nerve degeneration (area designated within arrows). (B) Axons from wild-type nerves do not show this swelled dense membranous axonal morphology. Two classes of axonal accumulations were observed in *robl*^{z} hemizygotes: (C) small single component (small clear vesicles) axonal accumulations and (D) larger multi-component axonal accumulations. (E) Severely sluggish *robl*^{z} hemizygous larvae showed increased axonal loss and degeneration. (F) All *robl*^{z} homozygous larvae consistently showed a high degree of axonal loss and nerve degeneration. Bars: (A, B, E, and F) 500 nm; (C and D) 200 nm.

nent accumulations contain almost exclusively small clear vesicles and tend to be smaller on average than the multicomponent accumulations. These small clear vesicles may represent a class of cargo that is particularly sensitive to retrograde transport failure in *robl* mutants. In support of this idea, when the synaptic area is examined by EM, there is an approximate twofold increase in the number of similar appearing small clear vesicles observed (data not shown).

The *robl* mutants also have severe axonal loss and nerve degeneration that is not observed in *khc* mutants, despite the fact that *khc* mutant axonal swellings are more numerous and on average twice the size of those observed in *robl* (Hurd and Saxton, 1996). All observed *robl*^{z} hemizygous larvae show at least mild axonal loss (Fig. 6 A). When the segmental nerves from the most severely sluggish *robl*^{z} hemizygous larvae are analyzed by EM, extensive axonal loss and nerve degeneration is observed (Fig. 6 E). Furthermore, the segmental nerves from *robl*^{z} homozygous larvae always show extensive axonal loss and nerve degeneration (Fig. 6 F). The basis for this axonal loss and nerve degeneration is unclear; however, we have observed a few large multilamellae structures (~1/10 nerve diameter) indicating a possible phagocytic component to the axonal loss and nerve degeneration (data not shown).

roadblock Is a Severe Mitotic Mutant and Female Sterile Mutation

The first indication of a mitotic defect in *robl* mutants was the observation of a complete absence of the mitotically active tissues (imaginal tissues) in *robl*^{z} homozygous larvae. Additionally, *robl*^{z} hemizygous and *robl* null animals that survive into late pupal stages, demonstrate rough pupal eyes (Fig. 7 L), missing bristles (data not shown), and reduced size of imaginal tissue (data not shown). These observations are consistent with a mitotic defect in *Drosophila*.

To examine the mitotic defect further, third instar untreated (no hypotonic or colchicine treatment) larval brain squashes were performed. This procedure permits observation of dividing neuroblasts within the larval central nervous system by staining with a fluorescent DNA dye and allows quantitation and characterization of the mitotic figures. The analysis revealed significant mitotic defects in *robl*^{z} hemizygous larvae. Numerous polyploid mitotic fig-

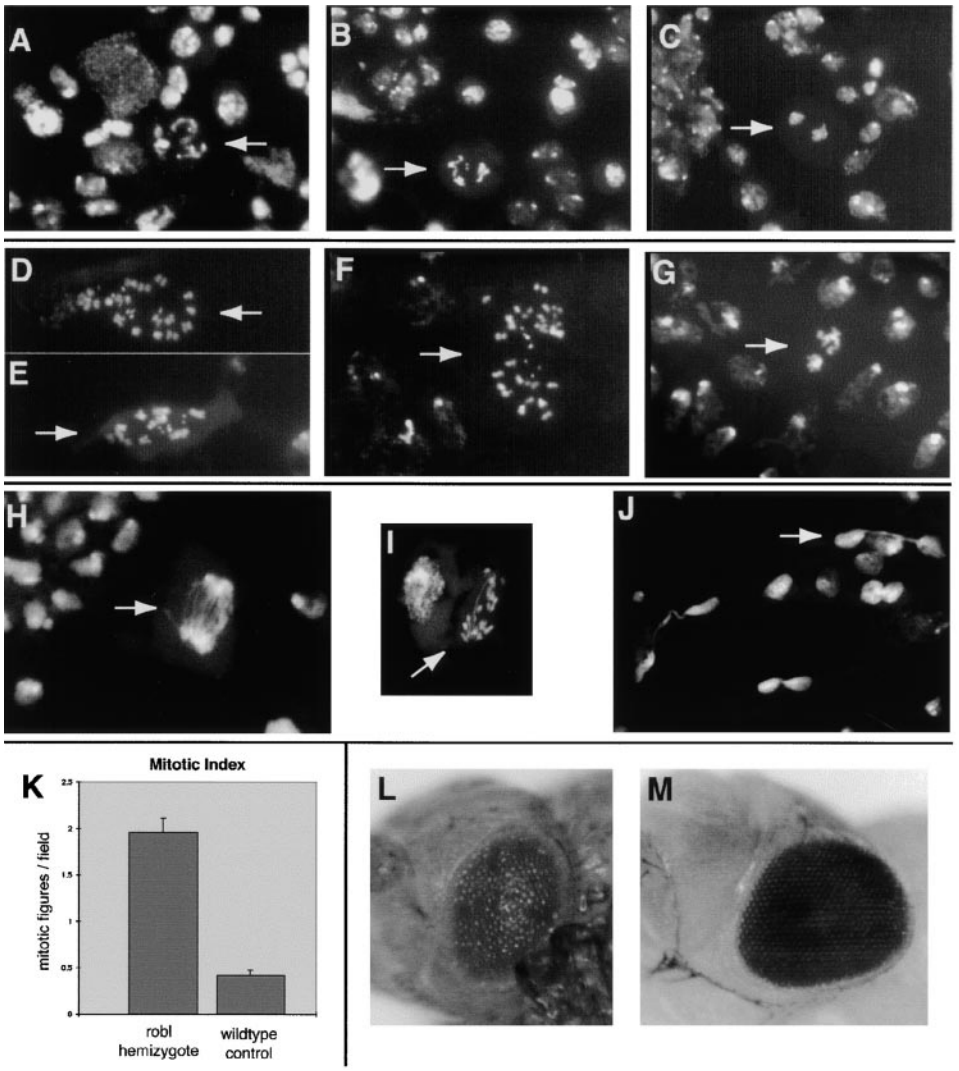

Figure 7. Severe mitotic defects were revealed in *robl* mutants examined by third instar larval brain squash analysis. Examples of typical wild-type mitotic figures are shown (designated by arrows): (A) a normal prometaphase figure, (B) a normal metaphase figure, and (C) a normal anaphase figure. Multiple abnormal mitotic figures are observed in *robl*^{z} hemizygotes, including (designated by arrows): (D and E) aneuploid figures, (F) aneuploid figures with hypercondensed chromosomes, and (G) mutant anaphase figures with hypercondensed chromosomes disorganized around the presumptive poles. Mitotic figures are infrequently found in *robl*^{z} homozygotes such as (designated by arrows): (H) a mutant anaphase structure with severe chromosome bridging, (I) another anaphase structure with a lagging chromosome and a single chromosome bridge, and (J) apparent telophase bridging. (K) The mitotic index of *robl*^{z} hemizygotes is about five times that of wild type, the error bars indicate the SEM. *robl*^{z} hemizygotes are late pupal lethal, when dissected from their pupal cases they show (L) rough pupal eyes. (M) A wild-type pupal eye is shown for comparison.

ures were observed (Fig. 7, D and E). Additionally, many of the polyploid figures showed hypercondensation of their chromosomes (Fig. 7 F). Abnormal anaphase figures were also observed with hypercondensed chromosomes and disorganization of the chromosomes around the presumptive poles (Fig. 7 G). As anticipated, since the mutant survives until late pupal stages, apparently normal mitotic figures were also observed (not shown). The mitotic index in this mutant is fivefold higher than wild type (Fig. 7 K). This increased mitotic index is due to an increased number of figures from all mitotic phases counted (prometaphase, metaphase, and anaphase). An elevated mitotic index for all phases, coupled with the variety of defective structures suggests defects in multiple stages of mitosis.

Larval brain squash analysis on the *robl*^{z} homozygotes also revealed a profound mitotic defect; in addition to the lack of imaginal tissue, there is a striking absence of prometaphase and metaphase mitotic figures. Only infrequent defective anaphase and telophase figures are seen. The few anaphase figures have severe bridging and lagging chromosomes (Fig. 7, H and I). In addition, we observe apparent telophase bridging in which DNA has become trapped between two dividing nuclei (Fig. 7 J). The failure to observe any prometaphase or metaphase figures prompted us to perform a larval brain squash on colchicine-treated brains. This procedure, which blocks cells in metaphase, resulted in an approximate doubling of the observed number of metaphase figures and a decrease in the observed frequency of postmetaphase figures in wild-type controls. However, in *robl*^{z} homozygotes, we never observed a prometaphase or metaphase figure in treated third instar larval brains, yet the low frequency of observed defective anaphase and telophase figures remained unchanged from untreated brains. These data strongly suggest that third instar *robl*^{z} homozygote larvae lack cells capable of division and the few figures observed represent cells arrested in mitosis.

Female *robl*^{z} hemizygous flies rescued to adulthood by the 6xHis-tagged cDNA construct under heat shock promoter control show a female sterile phenotype. However, this same allelic combination is fully rescued by the *robl* genomic rescue construct, presumably under native *robl* promoter control. Female sterility is commonly observed in mutants of cytoplasmic dynein components in *Drosophila* (Phillis et al., 1996; McGrail and Hays, 1997). Attempts to rescue the *robl* sterility phenotype by giving the cDNA-rescued females mild heat shock (to induce expression of *robl*) failed. Since the genomic construct fully rescues the female fertility defect, female sterility is likely a real *robl* mutant phenotype; *robl* cDNA under heat shock control is likely failing to provide appropriate levels of robl protein in the needed cells because of the inadequacy of non-native promoter control.

roadblock and a Mammalian robl/LC7-like Protein Are Associated with Cytoplasmic Dynein

Previously, the highly conserved LC8 protein and Tctex1 were found in both cytoplasmic and flagellar dyneins. The *robl* mutant phenotypes and the identification of a homologous sequence in organisms lacking motile cilia/flagella (*C. elegans*), raised the obvious possibility that robl/LC7-like proteins may be present in cytoplasmic dynein. Accordingly, we examined samples from the stepwise ATP-dependent microtubule affinity purification of cytoplasmic dynein from rat brain homogenates for the presence of a robl/LC7-like protein (Fig. 8 A). The R7178 antibody detected a single band of M_r ~12,000 in the initial microtubule pellet. Some robl/LC7, and a similar fraction of IC74, remained in the supernatant. Most of the robl/LC7 protein co-purified with microtubules through a buffer wash and GTP elution. Some of the protein was eluted from microtubules with ATP and nearly all of the remainder could be stripped by treatment with 1 M NaCl. In contrast, most IC74 was ATP-eluted. We previously observed that different DLCs do not show precisely the same pattern during elution from microtubules, perhaps because they mark specific subsets of cytoplasmic dynein with distinct microtubule binding characteristics (King et al., 1996a, 1998). To further address the association of the robl/LC7-like protein with cytoplasmic dynein, the ATP eluate was sedimented through a 5–20% sucrose gradient. Immunological analysis of the resulting fractions revealed that the robl/LC7-like protein sedimented at ~18 S and precisely copurified with the IC74 component of cytoplasmic dynein (Fig. 8 B).

To confirm this association, cytoplasmic dynein, dynactin, and kinesin from rat brain homogenates and cytoplasmic dynein from *Drosophila* embryo homogenates were immunoprecipitated with specific mAbs. The robl/LC7-like protein was pelleted only in the cytoplasmic dynein samples, no association was seen with dynactin, kinesin, or the bead controls (Fig. 8, C and D). The 6883 antiserum raised against the *Drosophila* robl protein detected a band of M_r ~12,000 from *Drosophila* embryonic and larval homogenates. This band was not present in homogenates from *robl* null larvae, indicating that the band seen by this antibody is the product of the *robl* gene (Fig. 8 E). These results demonstrate that a robl/LC7-like protein is indeed a component of cytoplasmic dynein from *Drosophila* and mammalian brain.

Discussion

We have identified a new family of axonemal- and cytoplasmic dynein–associated proteins. This family was identified by two independent means: the biochemical isolation and cloning of the *Chlamydomonas* dynein–associated LC7 polypeptide and the identification and cloning of a *Drosophila* axonal transport mutant, *roadblock*. Our discovery of a new family of DLCs with roles in axonal transport, flagellar motility, and mitosis has intriguing implications.

The Structural Organization of Dyneins

With this report, all the known components of *Chlamydomonas* outer arm dynein have now been sequenced and a complete list of the properties of outer dynein arm–associated DLCs can be made (Fig. 9 A). The outer dynein arm consists of three heavy chains that form the globular heads and stems of the particle. Each heavy chain is tightly associated with one or more light chains. Located at the

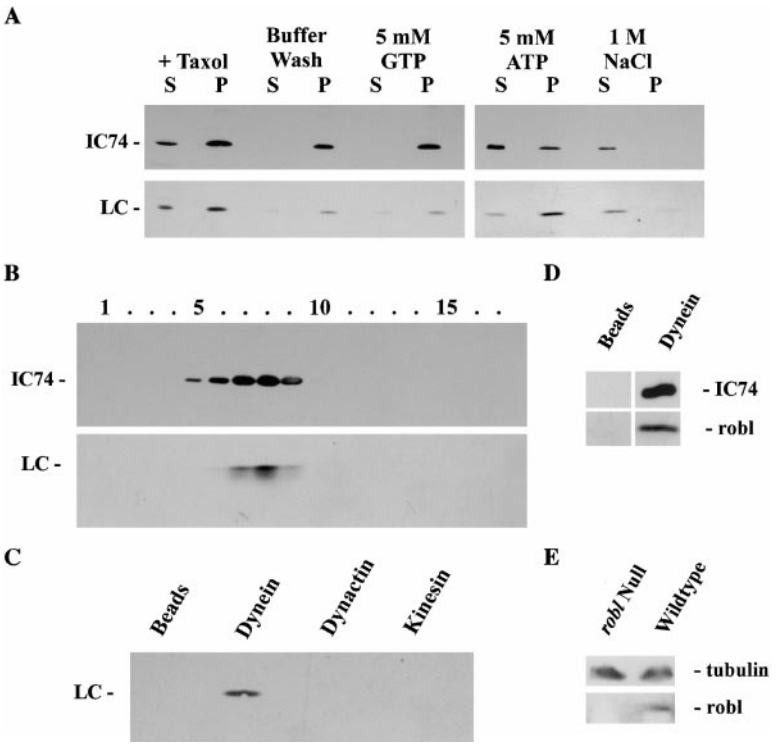

Figure 8. A robl/LC7-like protein is present in cytoplasmic dynein. (A) Western blot analysis was performed on samples from the fractionation of a rat brain homogenate. Blots were probed with mAb 74-1 and the R7178 rabbit polyclonal to detect IC74 of cytoplasmic dynein and the M_r ~12,000 robl/LC7-like protein, respectively. (B) Rat brain proteins eluted from microtubules with ATP were sedimented in a 5–20% sucrose gradient. Samples were probed with the 74-1 and R7178 antibodies. The robl/LC7-like protein precisely comigrates with IC74 of cytoplasmic dynein. (C) Rat brain homogenate immunoprecipitates of cytoplasmic dynein (antibody 74-1), kinesin (antibody H-2), dynactin (antibody 50-1), and a bead control were probed with the R7178 antibody. The robl/LC7-like protein is detectable only in the cytoplasmic dynein (IC74) sample. (D) *Drosophila* embryo immunoprecipitates of cytoplasmic dynein (antibody 74-1) or the bead control were probed with the 6883 anti-robl antibody and 74-1 anti-IC74 antibody. The roadblock protein was only precipitated in the cytoplasmic dynein (IC74) sample. (E) Equally loaded *Drosophila robl* null and wild-type larval homogenates were probed with the 6883 anti-robl antibody and with the 3A5 anti-tubulin antibody. The roadblock protein is undetectable in the *robl* null larvae, whereas tubulin is detected at about equal levels in null and wild-type larvae.

base of the structure are two intermediate chains (IC1 and IC2) and several additional light chains including a member of the Tctex1 protein family (LC2) together with multiple copies of the LC8 polypeptide and its homologue LC6. The LC7 protein is not tightly associated with any heavy chain and appears to form part of the intermediate–light chain complex located near the base of the particle (Mitchell and Rosenbaum, 1986).

Examination of outer armless mutants revealed that a very small amount of the LC7 protein was still incorpo-

A OUTER ARM DYNEIN LIGHT CHAINS

Light Chain	Nominal (Actual) Mass Da	Known Interactions	Properties
LC1	22,000 (22,150)	γ HC	Leucine-rich repeat protein
LC2	20,000 (15,882)	IC/LC complex	Tctex2 homologue
LC3	19,000 (17,364)	β HC	Thioredoxin-like
LC4	18,000 (17,787)	γ HC	Ca^{2+}-binding EF hand protein
LC5	16,000 (14,179)	α HC	Thioredoxin-like
LC6	14,000 (13,856)	IC/LC complex	LC8 homologue
LC7	11,000 (11,928)	IC/LC complex	Roadblock homologue
LC8	8,000 (10,321)	IC/LC complex	Highly conserved (in multiple complexes)

B MODEL OF CYTOPLASMIC DYNEIN ORGANIZATION

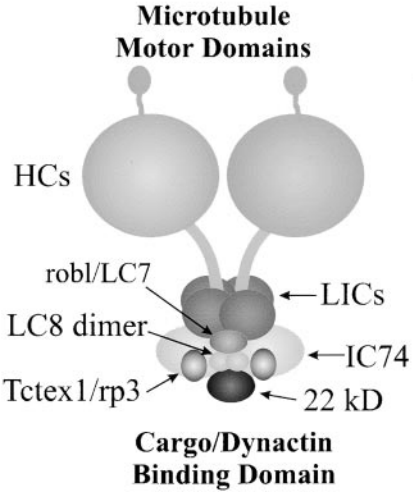

Cytoplasmic Dynein Associated Proteins	Homologous Axonemal Proteins
IC74	Outer Arm ICs
LIC	none identified
22 kDa	*uncloned*
Tctex1/rp3	Inner Arm light chain
robl/LC7	Outer Arm LC7
10 kDa/LC8	Outer Arm LC8

Figure 9. Summary of dynein-associated proteins. (A) A complete table of outer dynein arm–associated light chains is shown. The nominal mass refers to the M_r determined by SDS-PAGE analysis; actual predicted mass of the proteins is given parenthetically. Previous work has elucidated biochemical interactions amongst these proteins. (B) A model of cytoplasmic dynein organization is shown. The cytoplasmic dynein particle is built around two heavy chains that form the stems and globular heads of the complex. Associated with the stems are a series of accessory proteins including: two IC74 intermediate chains that mediate dynein–dynactin interactions, two copies of the Tctex1 light chain (or of the related rp3 protein), one dimer of the highly conserved 10 kD/LC8 DLC (LC8 dimer), and a 22-kD polypeptide (the location of which is speculative). The present study indicates that cytoplasmic dynein also contains a robl/LC7-like protein that, by analogy with flagellar outer arm dynein, is located at the base of the dynein particle. A table of known proteins associated with cytoplasmic dynein is given; the majority are conserved in axonemal dyneins.

rated into the axoneme. The origin of this pool remains unclear at present. It did not appear to derive from inner arm I1 as it could not be detected in salt extracts of axonemes lacking outer arms. It may represent a small pool of LC7 that is mistransported to the axoneme in the absence of the remainder of the outer arm. Alternatively, it may be associated with some other axonemal enzyme such as the DHC1b-like dynein that is responsible for retrograde intraflagellar transport (Pazour et al., 1999; Porter et al., 1999).

The cytoplasmic dynein particle is built around two ~520-kD heavy chains that form the stems and globular heads of the complex. Associated with the stems are a series of accessory proteins (Fig. 9 B). These are now known to include two IC74s, two copies of the Tctex1 light chain (or of the related rp3 protein), one dimer of the highly conserved LC8 protein, and perhaps a 22-kD polypeptide (the position of which is speculative). The present study indicates that cytoplasmic dynein also contains a robl/LC7-like protein. Since axonemal and cytoplasmic dyneins utilize homologous intermediate chain genes, it is likely that robl/LC7 associates with IC74. By analogy with flagellar outer arm dynein, we propose a cytoplasmic dynein organizational model where robl/LC7 is located at the base of the dynein particle (Fig. 9 B).

Cellular Functions that Require the robl/LC7 Family of Proteins

Previous work has provided strong evidence that cytoplasmic dynein plays an important role in retrograde axonal transport (for review see Hirokawa, 1998). Recent work in *Drosophila* has directly demonstrated that cytoplasmic dynein and dynactin play essential roles in retrograde axonal transport (Martin, M.A., personal communication). The distal enrichment of axonal accumulations that we observe in *robl*^{z} mutants is consistent with a defect in axonal transport that initiates at the synapse. One intriguing explanation for the nerve degeneration seen in *robl* mutants is a failure of the retrograde transport pathway mediating the transport of neurotrophic signals from the synapse to the neuronal cell body (Johanson et al., 1995; Bhattacharyya et al., 1997). The massive axonal loss and degeneration seen in *robl* mutants, but not in anterograde axonal transport mutants (such as *khc*), may indicate a specific inability of these factors to reach the cell body in *robl* mutants. In this context, it is striking that a subset of axonal swellings in *robl* mutants are filled predominantly with small vesicles (Fig. 6 C). This observation is consistent with recent work suggesting a distinct class of small vesicles, resembling transport vesicles, may be the carrier of the retrograde neurotrophic signal of nerve growth factor–activated receptor tyrosine kinase, TrkA (Grimes et al., 1997). Together, these data demonstrate that dynein is required for retrograde axonal transport in vivo.

Dynein is also thought to play a role in chromosome alignment and mitotic spindle assembly (Eshel et al., 1993; Li et al., 1993; Merdes et al., 1996). Overexpression of the p50 subunit of dynactin disrupted chromosome alignment, causing cells to accumulate in a prometaphase-like state (Echeverri et al., 1996). Additionally, anti-dynein antibody injection experiments blocked the formation of spindles in prophase (Vaisberg et al., 1993). The excessive number of chromosomes observed in aneuploid mitotic figures from *robl* mutants suggests a role for dynein in ensuring proper chromosome inheritance. However, the lack of prometaphase and metaphase figures in *robl*^{z} homozygotes, and an accumulation of defective anaphase and telophase figures, suggests that *robl*-dependent dynein function in metaphase spindle alignment and assembly is not required for entry into anaphase. *ZW10* mutants, which fail to localize dynein to the kinetochore, also exhibit anaphase defects, and has led to the suggestion that an absence of kinetochore-associated dynein function may allow a bypass of the wait anaphase checkpoint (Starr et al., 1998).

A role for dynein in the later stages of mitosis remains controversial. Cytoplasmic dynein heavy chain antibody injection experiments in mammalian cells failed to identify a role for dynein in anaphase chromosome movements (Vaisberg et al., 1993). Yet, dynein has been implicated in anaphase B spindle elongation in *Saccharomyces cerevisiae* (Saunders et al., 1995). The anaphase and telophase chromosome bridging and chromosome lagging in *robl* mutants supports a role for dynein in anaphase chromosome segregation. A possible explanation for the apparent late mitotic phenotype observed when *robl* is disrupted may be redundant mitotic motors. In fact, it is only in the triple motor mutant (*Cin8p Kip1p Dyn1p*) of *S. cerevisiae* that the role of dynein in anaphase B spindle elongation is revealed (Saunders et al., 1995). Perhaps complete loss of dynein function (expected for heavy chain mutants and anti–heavy chain injection experiments) allows redundant motors to perform dynein's role in chromosome segregation. However, a mutation of the dynein-associated protein robl/LC7 may not abolish dynein function and instead result in aberrant dynein activity, which could interfere with the ability of redundant motors to compensate. Alternatively, the anaphase defects of *robl* mutants may result from pre-anaphase mitotic spindle assembly defects that are not detected by checkpoint controls.

ESTs belonging to two mammalian robl/LC7-like gene classes have been found from a wide assortment of embryonic, adult, and germline tissues (Fig. 4 A). We identified >100 independent human ESTs in dbEST that encode a robl/LC7-like gene belonging to the first class (e.g., accession number hum424E02B). These ESTs are found from a wide array of tissues with unique and heavy intracellular transport needs such as: neural tissues (fetal and adult brain and retina), tissues with a heavy transcytosis burden (liver, spleen, kidney, placenta, and breast), a tissue involved in pigment dispersion (melanocyte), and mitotically active tissues (fetal and tumor tissues). Also, the rat robl/LC7-like gene from this first class was identified in the NCBI GenBank as being expressed in light-stimulated visual cortex (accession number 3288881). The robl/LC7-like gene identified by nine independent human ESTs of the second class (e.g., accession number AA446298) were found in a smaller subset of tissue types. This second class is found in human testes (6 of 9 clones) and tumor tissues (germ cell and kidney tumor tissues). Perhaps the testes expression may indicate a role for the second class with axonemal dynein, whereas the broad tissue expression may indicate a role for the first class with cytoplasmic dynein.

Together, the genetic and expression analyses suggest

that the robl/LC7 family is important for many aspects of intracellular transport. In *Drosophila*, the mutant phenotypes found thus far suggest that the *robl* gene is required for axonal transport and mitosis. In addition, the female sterility defect seen in some genetic combinations suggests a role for *robl* in oocyte development. This finding is consistent with previous evidence that dynein plays a role in oocyte differentiation in *Drosophila* (McGrail and Hays, 1997). In *Chlamydomonas*, the presence of LC7 in outer arm axonemal dynein suggests a role in flagellar motility. Finally, the expression inferred from human EST tissue sources within non-neural quiescent adult human tissues suggests that robl/LC7-like proteins may have a wider role than has been suggested thus far by the *Drosophila* mutant phenotypes.

Possible Roles of the robl/LC7 Family in Dynein Function

Our work on robl/LC7 adds to a growing body of evidence supporting modulatory roles for DLC proteins in dynein-mediated movements. Specifically, the observation that DLC phenotypes are not as severe as dynein heavy chain phenotypes, the structural placement of DLCs at key positions in dynein, and the nonequivalent phenotypes among DLC mutants, supports this view. For example, other than female sterility, *robl* mutants have no apparent phenotypic similarities to the 10-kD/LC8 DLC (*ddlc1*) mutants in *Drosophila* (Dick et al., 1996; Phillis et al., 1996). In addition, some evidence suggests that Tctex1 associates with only a subset of cytoplasmic dynein, indicating it is used for only a subset of dynein's functional roles (Tai et al., 1998). Intriguingly, the Tctex1-related protein rp3 may be associated with a cytoplasmic dynein population that does not contain Tctex1 (King et al., 1998). It is unclear whether each DLC plays a specific role in a subset of dynein functions or whether each DLC contributes generically to the functional roles of dynein.

In view of the dynein intermediate chains' possible structural role in linking motor activity to cargo binding activity, they may be a key regulatory target of the dynein complex. For example, IC74 mediates the binding of dynein to dynactin via a direct interaction with the $p150^{glued}$ subunit (Karki and Holzbaur, 1995). Interestingly, by analogy to homologous outer arm–associated proteins, all cloned cytoplasmic DLCs (including robl/LC7) are thought to associate with IC74 (Fig. 9 B). Since highly homologous DLCs are shared between the major dynein classes it seems likely that their functions in axonemal and cytoplasmic dyneins are also homologous. Some DLCs do not seem to provide strong dynein structural interactions based on the somewhat weaker interactions of LC7 and LC2 with outer arm dynein intermediate chains (Mitchell and Rosenbaum, 1986). One possibility is that some DLCs provide interaction sites for shared soluble regulatory factors that modulate the cargo binding activity of the dynein intermediate chains.

In support of a modulatory role for *robl*, there is evidence that loss of *robl* does not eliminate dynein function. For example, previous clonal analysis of the null allele $robl^{l(2)k10408}$ (before cloning of the gene) showed reduced clone size but a normal frequency of clone generation (Roch et al., 1998). However, clonal analysis of a strong cytoplasmic dynein heavy chain allele found a complete absence of clones in most flies and only a few small clones in the wing and abdomen observed in some flies (Gepner et al., 1996). Together these experiments suggest that whereas the *dynein heavy chain* gene is required for cell viability, cells can accomplish all minimally required cell autonomous dynein roles in the absence of *robl*. Furthermore, homozygous third instar *robl* null larvae have no detectable robl protein by Western analysis (Fig. 8 E). Despite an absence of the robl protein, these *robl* null larvae continue to develop to the late pupal stages. Together, these data suggest that cytoplasmic dynein remains at least partially functional in the absence of *robl*.

There is evidence that *robl* actively modulates dynein activity. The $robl^{z}$ homozygotes have a significantly stronger phenotype than *robl* nulls, exhibiting a complete absence of imaginal tissue, and eventually complete posterior larval paralysis and larval lethality. Yet, $robl^{z}$/null animals are phenotypically similar to *robl* null animals, exhibiting only a slight reduction in the size of imaginal tissue, distal larval sluggishness without eventual paralysis, and survival to the late pupal stages. The accumulations of axonal cargoes in microtubule-based motor mutants in *Drosophila* may be caused by decreased processivity of cargo whose transport is directly dependent on the motor affected by the mutation, resulting in a buildup of other axonal cargo around this stalled cargo. The observed correlation of fewer axonal accumulations occurring in larvae with more copies of the $robl^{z}$ allele may suggest that fewer cargoes are entering the axons in these alleles. Thus, fewer accumulations may occur because there is less robl-dependent cargo within the axons. The concentration dependence of the $robl^{z}$ phenotype suggests that this *robl* allele interferes actively and directly with dynein function. Furthermore, since $robl^{z}$ can result in phenotypes worse than *robl* nulls, this aberrant DLC apparently has the ability to alter the functions of the dynein holoenzyme.

We thank Kevin Pfister (University of Virginia Health Science Center, Charlottesville, VA) for cytoplasmic dynein samples, the University of California San Diego (UCSD) Immunocytochemistry/EM Core and Marilyn Farquhar (UCSD) for use of EM facilities, and MaryAnn Martin and Bill Saxton (both from Indiana University, Bloomington, ID) for discussions and sharing of unpublished work. We express sincere appreciation to Charles Zuker, Edmund Koundakjian, David Cowan, and Robert Hardy (all from UCSD) for providing the balanced EMS mutant lines used to identify $robl^{z}$.

A. Bowman is supported by the UCSD Pharmacology Training Grant and is a Markey Research Fellow. L. Goldstein is an investigator of the Howard Hughes Medical Institute. This study was supported by GM35252 (to L. Goldstein) and GM51293 (to S. King) from the National Institutes of Health.

Submitted: 28 January 1999
Revised: 26 May 1999
Accepted: 4 June 1999

References

Beckwith, S.M., C.H. Roghi, B. Liu, and N.R. Morris. 1998. The "8-kD" cytoplasmic dynein light chain is required for nuclear migration and for dynein heavy chain localization. *J. Cell Biol.* 143:1239–1247.

Bhattacharyya, A., F.L. Watson, T.A. Bradlee, S.L. Pomeroy, C.D. Stiles, and R.A. Segal. 1997. Trk receptors function as rapid retrograde signal carriers in the adult nervous system. *J. Neurosci.* 17:7007–7016.

Crepieux, P., H. Kwon, N. Leclerc, W. Spencer, S. Richard, R. Lin, and J. His-

cott. 1997. I kappaB alpha physically interacts with a cytoskeleton-associated protein through its signal response domain. *Mol. Cell. Biol.* 17:7375–7385.

Dick, T., K. Ray, H.K. Salz, and W. Chia. 1996. Cytoplasmic dynein (ddlc1) mutation cause morphogenetic defects and apoptotic cell death in *Drosophila melanogaster*. *Mol. Cell. Biol.* 16:1966–1977.

Dillman, J.F., and K.K. Pfister. 1994. Differential phosphorylation in vivo of cytoplasmic dynein associated with anterogradely moving organelles. *J. Cell Biol.* 127:1671–1681.

Echeverri, C.J., B.M. Paschal, K.T. Vaughan, and R.B. Vallee. 1996. Molecular characterization of the 50-kD subunit of dynactin reveals function for the complex in chromosome alignment and spindle organization during mitosis. *J. Cell Biol.* 132:617–633.

Eshel, D., L.A. Urrestarazu, S. Vissers, J.-C. Jauniaux, J.C. van Vliet-Reedijk, R.J. Planta, and I.R. Gibbons. 1993. Cytoplasmic dynein is required for normal nuclear segregation in yeast. *Proc. Natl. Acad. Sci. USA*. 90:11172–11176.

Gepner, J., M. Li, S. Ludman, C. Kortas, K. Boylan, S.J.P. Iyadurai, M. McGrail, and T.S. Hays. 1996. Cytoplasmic dynein function is essential in *Drosophila melanogaster*. *Genetics*. 142:865–878.

Gindhart, J.G., C.J. Desai, S. Beushausen, K. Zinn, and L.S.B. Goldstein. 1998. Kinesin light chains are essential for axonal transport in *Drosophila*. *J. Cell Biol.* 141:443–454.

Gonzalez, C., and D.M. Glover. 1993. Techniques for studying mitosis in *Drosophila*. *In* The Cell Cycle: A Practical Approach. P. Fantes and R. Brookes, editors. Oxford University Press, Oxford, UK. 163–168.

Grimes, M.L., E. Beattie, and W.C. Mobley. 1997. A signaling organelle containing the nerve growth factor-activated receptor tyrosine kinase, TrkA. *Proc. Natl. Acad. Sci. USA*. 94:9909–9914.

Harrison, A., P. Olds-Clarke, and S.M. King. 1998. Identification of the *t* complex-encoded cytoplasmic dynein light chain Tctex1 in inner arm I1 supports the involvement of flagellar dyneins in meiotic drive. *J. Cell Biol.* 140:1137–1147.

Hirokawa, N. 1998. Kinesin and dynein superfamily proteins and the mechanism of organelle transport. *Science*. 279:519–526.

Holleran, E.A., S. Karki, and E.L.F. Holzbaur. 1998. The role of the dynactin complex in intracellular motility. *Int. Rev. Cytol.* 182:69–109.

Hurd, D.D., and W.M. Saxton. 1996. Kinesin mutations cause motor neuron disease phenotypes by disrupting fast axonal transport in *Drosophila*. *Genetics*. 144:1075–1085.

Jaffrey, S.R., and S.H. Snyder. 1996. PIN: an associated protein inhibitor of neuronal nitric oxide synthase. *Science.* 274:774–777.

Johanson, S.O., M.F. Crouch, and I.A. Hendry. 1995. Retrograde axonal transport of signal transduction proteins in rat sciatic nerve. *Brain Res.* 690:55–63.

Kagami, O., M. Gotoh, Y. Makino, H. Mohri, R. Kamiya, and K. Ogawa. 1998. A dynein light chain in sea urchin sperm flagella is a homolog of mouse Tctex1, which is encoded by a gene of the t complex sterility locus. *Gene.* 211:383–386.

Karki, S., and E.L. Holzbaur. 1995. Affinity chromatography demonstrates a direct binding between cytoplasmic dynein and the dynactin complex. *J. Biol. Chem*. 270:28806–28811.

King, S.M., and R.S. Patel-King. 1995a. Identification of a Ca^{2+}-binding light chain within *Chlamydomonas* outer arm dynein. *J. Cell Sci.* 108:3757–3764.

King, S.M., and R.S. Patel-King. 1995b. The M_r 8,000 and 11,000 outer arm dynein light chains from *Chlamydomonas* flagella have cytoplasmic homologues. *J. Biol. Chem*. 270:11445–11452.

King, S.M., E. Barbarese, J.F. Dillman, R.S. Patel-King, J.H. Carson, and K.K. Pfister. 1996a. Brain cytoplasmic and flagellar outer arm dyneins share a highly conserved M_r 8,000 light chain. *J. Biol. Chem*. 271:19358–19366.

King, S.M., J.F. Dillman, S.E. Benashski, R.J. Lye, R.S. Patel-King, and K.K. Pfister. 1996b. The mouse *t*-complex-encoded protein Tctex-1 is a light chain of brain cytoplasmic dynein. *J. Biol. Chem*. 271:32281–32287.

King, S.M., E. Barbarese, J.F. Dillman, S.E. Benashski, K.T. Do, R.S. Patel-King, and K.K. Pfister. 1998. Cytoplasmic dynein contains a family of differentially expressed light chains. *Biochemistry*. 37:15033–15041.

Li, Y.Y., E. Yeh, T. Hays, and K. Bloom. 1993. Disruption of mitotic spindle orientation in a yeast dynein mutant. *Proc. Natl. Acad. Sci. USA*. 90:10096–10100.

Lipshitz, H.D., D.A. Peattie, and D.S. Hogness. 1987. Novel transcripts from the *Ultrabithorax* domain of the bithorax complex. *Genes Dev*. 1:307–322.

Littleton, J.T., H.J. Bellen, and M.S. Perin. 1993. Expression of synaptotagmin in *Drosophila* reveals transport and localization of synaptic vesicles to the synapse. *Development.* 118:1077–1088.

McCaffery, J.M., and M.G. Farquhar. 1995. Localization of GTPases by indirect immunofluorescence and immunoelectron microscopy. *Methods Enzymol*. 257:259–279.

McGrail, M., and T.S. Hays. 1997. The microtubule motor cytoplasmic dynein is required for spindle orientation during germline cell division and oocyte differentiation in *Drosophila*. *Development*. 124:2409–2419.

Merdes, A., K. Ramyar, J.D. Vechio, and D.W. Cleveland. 1996. A complex of NuMa and cytoplasmic dynein is essential for mitotic spindle assembly. *Cell.* 87:447–458.

Milisav, I. 1998. Dynein and dynein-related genes. *Cell Motil. Cytoskel.* 39:261–272.

Mitchell, D.R., and J.L. Rosenbaum. 1986. Protein-protein interactions in the 18S ATPase of *Chlamydomonas* outer dynein arms. *Cell Motil. Cytoskel*. 6:510–520.

Olmsted, J.B. 1986. Analysis of cytoskeletal structures using blot-purified monospecific antibodies. *Methods Enzymol.* 134:467–472.

Paschal, B.M., H.S. Shpetner, and R.B. Vallee. 1991. Purification of brain cytoplasmic dynein and characterization of its in vitro properties. *Methods Enzymol*. 196:181–191.

Pazour, G.J., C.G. Wilkerson, and G.B. Witman. 1998. A dynein light chain is essential for the retrograde particle movement of intraflagellar transport (IFT). *J. Cell Biol*. 141:979–992.

Pazour, G.J., B.L. Dickert, and G.B. Witman. 1999. The DHC1b (DHC2) isoform of cytoplasmic dynein is required for flagellar assembly. *J. Cell Biol.* 144:473–481.

Pfister, K.K., R.B. Fay, and G.B. Witman. 1982. Purification and polypeptide composition of dynein ATPases from the *Chlamydomonas* flagella. *Cell Motil.* 2:525–547.

Phillis, R., D. Statton, P. Caruccio, and R.K. Murphey. 1996. Mutations in the 8 kDa dynein light chain gene disrupt sensory axon projections in the *Drosophila* imaginal CNS. *Development*. 122:2955–2963.

Piperno, G., and M.T. Fuller. 1985. Monoclonal antibodies specific for an acetylated form of α-tubulin recognize the antigen in cilia and flagella from a variety of organisms. *J. Cell Biol.* 101:2085–2094.

Piperno, G., and J.L. Luck. 1979. Axonemal adenosine triphosphatases from flagella of *Chlamydomonas reinhardtii:* purification of two dyneins. *J. Biol. Chem*. 254:3084–3090.

Porter, M.E., R.L. Bower, J.A. Knott, P. Byrd, and W. Dentler. 1999. Cytoplasmic dynein heavy chain 1b is required for flagellar assembly in *Chlamydomonas. Mol. Biol. Cell.* 10:693–712.

Roch, F., F. Serras, F.J. Cifuetes, M. Corominas, B. Alsina, M. Amoros, A. Lopez-Varea, R. Hernandez, D. Guerra, S. Cavicchi, J. Baguna, and A. Garcia-Bellido. 1998. Screening of larval/pupal P-element induced lethals on the second chromosome in *Drosophila melanogaster*: clonal analysis and morphology of imaginal discs. *Mol. Gen. Genet.* 257:103–112.

Saunders, W.S., D. Koshland, D. Eshel, I.R. Gibbons, and M.A. Hoyt. 1995. *Saccharomyces cerevisiae* kinesin- and dynein-related proteins required for anaphase chromosome segregation. *J. Cell. Biol*. 128:617–624.

Starr, D.A., B.C. Williams, T.S. Hays, and M.L. Goldberg. 1998. ZW10 helps recruit dynactin and dynein to the kinetochore. *J. Cell Biol*. 142:763–774.

Tai, A.W., J.Z. Chuang, and C.H. Sung. 1998. Localization of Tctex-1, a cytoplasmic dynein light chain, to the Golgi apparatus and evidence for dynein complex heterogeneity. *J. Biol. Chem*. 273:19639–19649.

Vaisberg, E.A., M.P. Koonce, and J.R. McIntosh. 1993. Cytoplasmic dynein plays a role in mammalian mitotic spindle formation. *J. Cell Biol.* 123:849–858.

Witman, G.B. 1986. Isolation of *Chlamydomonas* flagella and flagellar axonemes. *Methods Enzymol.* 134:280–290.

Yasuyama, K., T. Kitamoto, and P.M. Salvaterra. 1995. Localization of choline acetyltransferase-expressing neurons in the larval visual system of *Drosophila melanogaster. Cell Tissue Res.* 282:193–202.